Supplement of

High contribution of anthropogenic combustion sources to atmospheric inorganic reactive nitrogen in South China evidenced by isotopes

Tingting Li[1,2,4], Jun Li[*1,2], Zeyu Sun[3,4], Hongxing Jiang[1], Chongguo Tian[3], Gan Zhang[1,2]

[1]State Key Laboratory of Organic Geochemistry and Guangdong province Key Laboratory of Environmental Protection and Resources Utilization, Guangdong-Hong Kong-Macao Joint Laboratory for Environmental Pollution and Control, Guangzhou Institute of Geochemistry, Chinese Academy of Sciences, Guangzhou, 510640, China
[2]CAS Center for Excellence in Deep Earth Science, Guangzhou 510640, P. R. China
[3]Yantai Institute of Coastal Zone Research, Chinese Academy of Sciences, Yantai 264003, P. R. China
[4]University of Chinese Academy of Sciences, Beijing 100049, P. R. China
**Correspondence to*: Jun Li (junli@gig.ac.cn)

Contents:

Text S1 Chemical components analysis

OC/EC: OC and EC contents were analyzed by thermal-optical carbon analyzer (Sunset Laboratory Inc). One punch of 1.5 cm^2 filter samples was cut and put into the instrument. Blank samples were measured by same methods. Quality control standards (sucrose solutions) were dropped onto quartz membranes to dry and then the carbon content was tested in the same way to ensure that the instrument was stable before measurement and in the testing process.

Water-soluble ions: Na^+, K^+, Mg^{2+}, Ca^{2+}, NH_4^+, Cl^-, SO_4^{2-}, and NO_3^- were measured by ion chromatography. The blank samples were also analyzed following the same procedure for samples. Reagent blanks (ultrapure water) and quality control standards were measured every 10 samples to detect contamination and drift.

Isotopic analysis: The $\delta^{15}N\text{-}NO_3^-$ and $\delta^{18}O\text{-}NO_3^-$ values (‰) were corrected by multi-point correction (r^2=0.999) based on international standards (IAEA-NO_3, USGS32, USGS34, and USGS35) and $\delta^{15}N\text{-}NH_4^+$ was corrected by international standards (IAEA-N1, USGS25, and USGS26) (Sun et al., 2021; Zong et al., 2017).

Radioactive isotope analysis: ^{210}Pb and ^{7}Be were analyzed at Shenzhen University using high-purity γ spectrometer equipped with an HPGe detector (Jiang et al., 2021; Liu et al., 2020). ^{210}Pb in the atmosphere mainly comes from terrestrial sources and is effective indicator of the aerosols transport from continental surface. The $f(^{7}Be, ^{210}Pb)$ index is powerful to reveal the influence of atmospheric dynamic transport on variations in aerosol pollutants, and expressed as following equation (Jiang et al., 2021). Generally, the relatively high values of $f(^{7}Be, ^{210}Pb)$ index represented that the aerosol pollutants were influenced by long range transport from upper air.

$$f(^{7}Be,^{210}Pb) = \frac{[^{7}Be]}{[^{7}Be]+n[^{210}Pb]} \qquad \text{(S1)}$$

where $[^{7}Be]$ and $[^{210}Pb]$ are activity concentrations of ^{7}Be and ^{210}Pb, respectively, n is estimated as the ratio of standard deviation of $[^{7}Be]$ to $[^{210}Pb]$.

Trace gas: concentrations of trace gases (NO, NO_2, SO_2, O_3, and CO) were acquired from online equipment. The online equipment included a gas filter analyzer (Thermo Scientific, Model 48i) to measure CO, a pulse fluorescence analyzer (Thermo

Scientific, Model 43iTLE) to measure SO_2 and O_3, and a chemiluminescence apparatus (Thermo Scientific, Model 42iTL) to measure NO and NO_2.

Meteorological parameters: Temperature, relative humidity, wind speed, and atmospheric pressure were also acquired by a portable weather analyzer (WXT520, Vaisala, Finland). Trace gas concentrations and meteorological parameters were hourly data. In this study, average data of 24 hours through a sampling period were used.

Text S2 Source apportionment of NO_3^- and NH_4^+

Bayesian mixing model coupled with $\delta^{15}N\text{-}NO_3^-$ and $\delta^{18}O\text{-}NO_3^-$ were used to identify formation process and quantify the contribution of sources of NO_3^-. NO_3^- formation pathway mainly including ·OH and N_2O_5 channel, details shown in **Text S5**. Based on $\delta^{18}O\text{-}NO_3^-$, $\delta^{18}O\text{-}H_2O$ (-25‰-0‰), $\delta^{18}O\text{-}O_3$(90‰-122‰), and temperature coupled with Monte Carlo simulation nested in Bayesian mixing model (equations S2-S5, **Table S1**), the proportion of the contribution of ·OH formation pathway (γ) was estimated(Zong et al., 2017). According to the maximum γ, minimum γ, and temperature, the nitrogen fractionation value (εN) was calculated (equations S5-S8)(Zong et al., 2017). Then the potential sources of NOx were quantified by Bayesian mixing model coupled with εN, mixture of $\delta^{15}N\text{-}NO_3^-$, and sources of $\delta^{15}N\text{-}NOx$ shown in **Table S2a** (Zong et al., 2017).

$$[\delta^{18}O\text{-}NO_3^-] = \gamma \times [\delta^{18}O\text{-}NO_3^-]_{OH} + (1-\gamma) \times [\delta^{18}O\text{-}NO_3^-]_{H2O} = \gamma \times [\delta^{18}O\text{-}HNO_3]_{OH} + (1-\gamma) \times [\delta^{18}O\text{-}HNO_3]_{H2O} \quad (S2)$$

$$[\delta^{18}O\text{-}HNO_3]_{OH} = \frac{2}{3}[(\delta^{18}O\text{-}NO_2)]_{OH} + \frac{1}{3}[\delta^{18}O\text{-}OH]_{OH} = \frac{2}{3}\left[\frac{1000\times\left(18\alpha_{\frac{NO2}{NO}}-1\right)\left(1-f_{NO_2}\right)}{\left(1-f_{NO_2}\right)+\left(18\alpha_{\frac{NO2}{NO}}\times f_{NO_2}\right)} + [\delta^{18}O\text{-}NO_X]\right] + \frac{1}{3}[(\delta^{18}O\text{-}H_2O) + 1000 \times (18\alpha_{\frac{OH}{H2O}} - 1)] \quad (S3)$$

$$[\delta^{18}O\text{-}HNO_3]_{H2O} = \frac{5}{6}(\delta^{18}O\text{-}N_2O_5) + \frac{1}{6}(\delta^{18}O\text{-}H_2O) \quad (S4)$$

$$1000({}^{m}\alpha_{X/Y} - 1) = \frac{A}{T^4} \times 10^{10} + \frac{B}{T^3} \times 10^{8} + \frac{C}{T^2} \times 10^{6} + \frac{D}{T} \times 10^{4} \quad (S5)$$

$$\varepsilon N = \gamma \times \varepsilon(\delta^{15}N\text{-}NO_3^-)_{OH} + (1-\gamma) \times \varepsilon(\delta^{15}N\text{-}NO_3^-)_{H2O} = \gamma \times \varepsilon(\delta^{15}N\text{-}HNO_3)_{OH} + (1-\gamma) \times \varepsilon(\delta^{15}N\text{-}HNO_3)_{H2O} \quad (S6)$$

$$\varepsilon(\delta^{15}N\text{-}HNO_3)_{OH} = \varepsilon(\delta^{15}N\text{-}NO_2)_{OH} = 1000 \times \left[\frac{(15\alpha_{NO2/NO}-1)(1-f_{NO_2})}{(1-f_{NO_2})+(15\alpha_{NO2/NO}\times f_{NO_2})}\right] \quad (S7)$$

$$\varepsilon(\delta^{15}\mathrm{N\text{-}HNO_3})_{H_2O} = \varepsilon(\delta^{15}\mathrm{N\text{-}N_2O_5})_{H_2O} = 1000 \times \left(15\alpha_{N2O5/NO2} - 1\right) \quad \text{(S8)}$$

Where, γ is the contribution ratio of the isotopic fractionation through the reaction of NO_2 and photochemically produced ·OH, εN refers to N fractionation. $f$$NO_2$ is the fraction of NO_2 in the total NOx. The reported range of $f$$NO_2$ is from 0.2 to 0.95(Zong et al., 2017). $^{18}\alpha NO_2/NO$ and $^{18}\alpha OH/H_2O$ are the equilibrium isotope fractionation factors between NO_2 and NO and ·OH and H_2O, respectively.$^{15}\alpha NO_2/NO$ and $^{15}\alpha N_2O_5/NO_2$ are the equilibrium isotope fractionation factor between NO_2 and NO, and N_2O_5 and NO_2, respectively.

Table S1. Test constants of A, B, C, and D over the settled temperature range of 150−450K(Zong et al., 2017).

$^{m}\alpha_{X/Y}$	A	B	C	D
$^{15}NO_2/NO$	3.8834	-7.7299	6.0101	-0.17928
$^{15}N_2O_5/NO_2$	0.69398	-1.9859	2.3876	0.16308
$^{18}NO/NO_2$	-0.04129	1.1605	-1.8829	0.74723
$^{18}H_2O/OH$	2.1137	-3.8026	2.5653	0.59410

Table S2a. The estimation of δ^{15}N-NOx from various sources.

Source	δ^{15}N-NOx(‰)	Reference
Biomass burning	1.04	(Zong et al., 2017; Fibiger and Hastings, 2016; Zong et al., 2022)
Coal combustion	13.72	(Zong et al., 2017; Felix et al., 2015; Felix et al., 2012)
Mobile source	-7.25	(Zong et al., 2017; Walters et al., 2015)
Biogenic soil emission	-33.77	(Zong et al., 2017; Felix and Elliott, 2013)

Table S2b. The estimation of δ^{15}N-NH_3 from various sources.

Source	δ^{15}N-NH_3(‰)	Reference
Biomass burning	17.5	(Kawashima and Kurahashi, 2011; Xiao et al., 2020)
Coal combustion	-2.5	(Felix et al., 2013)
Urban traffic	6.6	(Walters et al., 2020)
Fertilizer	-28.3	(Bhattarai et al., 2021; Chang et al., 2016; Felix et al., 2013)
Livestock	-18.3	(Bhattarai et al., 2021; Chang et al., 2016; Felix et al., 2013)
Urban waste	-22.8	(Bhattarai et al., 2021; Chang et al., 2016)

IsoSource model coupled with mixture of δ^{15}N-NH_3 and sources of δ^{15}N-NH_3 shown in **Table S2b** were applied to quantify the NH_4^+ source. δ^{15}N-NH_3 in mixture was calculated by following equation.

$$\delta^{15}\mathrm{N}\text{-}\mathrm{NH_3} = \delta^{15}\mathrm{N}\text{-}\mathrm{NH_4^+} - \varepsilon(\mathrm{NH_4^+}\text{-}\mathrm{NH_3}) \times (1 - \mathrm{f}) \quad \text{(S9)}$$

Where, δ^{15}N-NH_3 and δ^{15}N-NH_4^+ represent the δ^{15}N values of NH_3 and NH_4^+, respectively. $\varepsilon(NH_4^+\text{-}NH_3)$ denotes the corresponding isotope enrichment factor, which is estimated as +33‰(Liu et al., 2018; Pan et al., 2016). The f value is the fraction of the initial NH_3 converted to the ion phase, which referenced the observed NH_3 and NH_4^+ in Guangzhou(Liao et al., 2014).

Text S3 Isotopic fractionation coefficient estimation between NH_3 and NH_4^+

Environmental temperature has influence on atmospheric NH_3 and NH_4^+ chemical processes and concentration(Kawashima and Kurahashi, 2011). Generally, the effect of temperature on atmospheric NH_3 results in a decrease in NH_3 concentration during the cold season and an increase during the warm season(Kawashima and Kurahashi, 2011). A linear fitting equation was observed between $NH_4^+/(NH_3+NH_4^+)$ and δ^{15}N-NH_4^+, and the absolute value of the slope (-32.41) approximated the isotope equilibrium

fractionation value (+33%) of NH_3 and NH_4^+ in the atmospheric environment, **equation (S4)**. In addition, the linear fitting results suggested that the lower the NH_4^+ proportion was, the heavier the δ^{15}N-NH_4^+ value (**Figure S2**), which was in line with the observed values in this study.

$$\delta^{15}\text{N-}NH_4^+ - \delta^{15}\text{N-}NH_3 = \Delta \quad \text{(S1)}$$

$$fNH_4^+ + fNH_3 = 1 \quad \text{(S2)}$$

$$\delta^{15}\text{N-}NH_4^+ * fNH_4^+ + (\delta^{15}\text{N-}NH_4^+ - \Delta) * (1 - fNH_4^+) = \delta^{15}\text{N} \quad \text{(S3)}$$

$$\delta^{15}\text{N-}NH_4^+ = -\Delta * fNH_4^+ + (\delta^{15}\text{N} + \Delta) \quad \text{(S4)}$$

Where, δ^{15}N-NH_4^+ and δ^{15}N-NH_3 was the δ^{15}N of atmospheric NH_4^+ and NH_3, fNH_4^+ and fNH_3 was the proportion of atmospheric NH_4^+ and NH_3, Δ was the equilibrium fractionation value between NH_4^+ and NH_3, and δ^{15}N was the sum of δ^{15}N-NH_4^+ and δ^{15}N-NH_3.

Text S4 The estimation of δ^{15}N-NH_4^+ from sugarcane leaf burning

The δ^{15}N in sugarcane leaf is 38‰ (Martinellia et al., 2002), which may consist N-NO_X and N-NH_3. The δ^{15}N-NOx from biomass burning is 1.04‰(Zong et al., 2017). According to the assumption of different proportion (from 5% to 95%) of N-NO_X and N-NH_3 from sugarcane leaf, shown **Table S3**. The mean value among the proportion (from 5% to 95%) of N-NH_4^+ in sugarcane leaf was 37.48‰. In addition, the δ^{15}N of particulate matters from biomass burning was 6.6‰ higher than that of biomass (Martinellia et al., 2002). Therefore, δ^{15}N-NH_4^+ from sugarcane leaf burning may be 44.08‰.

Table S3. The estimation of δ^{15}N-NH_3 in sugarcane leaf.

N-NOx in sugarcane leaf (%)	5	25	50	75	95
δ^{15}N in sugarcane leaf (‰)	38	38	38	38	38
δ^{15}N-NOx (‰)	1.04	1.04	1.04	1.04	1.04
Caculated results δ^{15}N-NH_3 (‰)	37.95	37.74	37.48	37.22	37.01

Text S5 The NO_3^- formation pathway

Once emitted into the atmosphere, NOx is oxidized to HNO_3 or NO_3^- via the

following chemical pathways (R1-R8) (Fang et al., 2011). In summary, NOx oxygen atoms are rapidly exchanged with O_3 in the NO/NO_2 cycle (R1-R3); ·OH radicals result in the oxidation of NO_2 to HNO_3 (R4; the ·OH pathway); NO_2 is oxidized by O_3 to produce NO_3 (R5), which subsequently combines with NO_2 to form N_2O_5 (R6), and then undergoes hydrolysis to form HNO_3 (R7), referred to as the O_3 pathway; and the generated HNO_3 combines with alkali to form NO_3^- (R8). Overall, the ·OH and O_3 pathways are the two fundamental oxidation pathways for NOx, generally exhibiting noticeable diurnal and seasonal variation(Elliott et al., 2007). Previous research has found that the ·OH pathway is more prevalent during the daytime and in summer, when the relative concentration of ·OH is higher. Conversely, the O_3 pathway is more dominant overnight and in winter, because N_2O_5 is thermally unstable(Hastings et al., 2003; Xiao et al., 2015). The O_3 in the troposphere has a higher $\delta^{18}O$ value (90‰-122‰), while $\delta^{18}O$-OH is lower (-25‰-0‰) (Zong, 2017). The $\delta^{18}O$-HNO_3 formed by the ·OH pathway is contributed by 2/3 O_3 and 1/3 ·OH (R4), while in N_2O_5 hydrolysis pathway after oxidation by O_3, the $\delta^{18}O$-HNO_3 is contributed by 5/6 O_3 and 1/6 H_2O (R5-R7). Therefore, the $\delta^{18}O$-NO_3^- formed through the ·OH pathway is lower than N_2O_5 pathway.

$$NO + O_3 \rightarrow NO_2 + O_2 \quad (R1)$$

$$NO_2 + hv \rightarrow NO + O \quad (R2)$$

$$O + O_2 \rightarrow O_3 \quad (R3)$$

$$NO_2 + \cdot OH \rightarrow HNO_3 \quad (R4)$$

$$NO_2 + O_3 \rightarrow NO_3 + O_2 \quad (R5)$$

$$NO_2 + NO_3 \rightarrow N_2O_5 \quad (R6)$$

$$N_2O_5 + H_2O \rightarrow 2HNO_3 \quad (R7)$$

$$HNO_3 + Alkali \rightarrow NO_3^- \quad (R8)$$

Figure S1-Figure S6

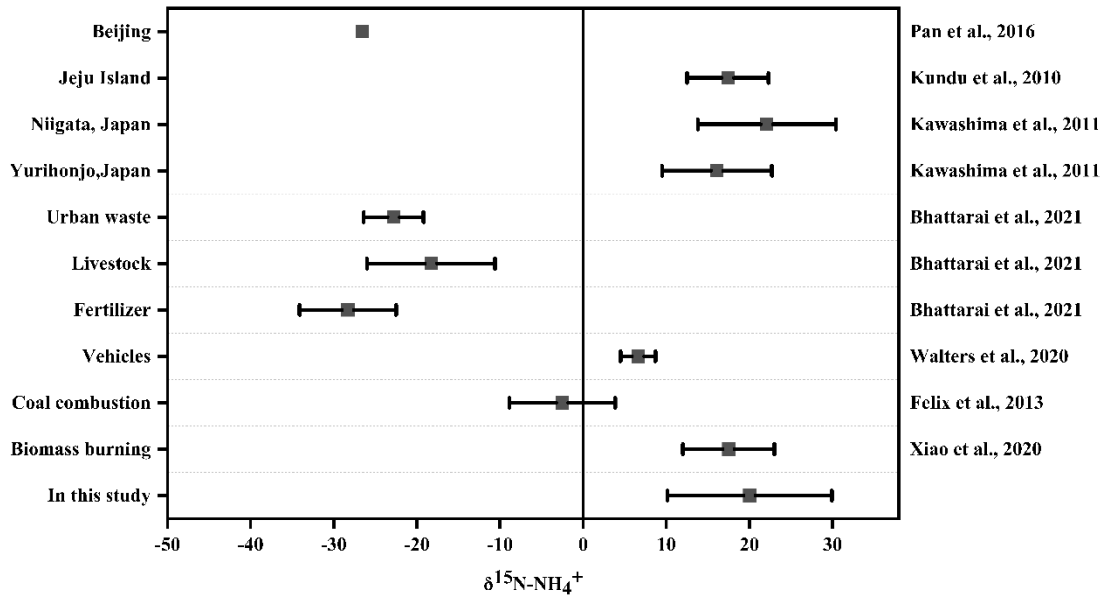

Figure S1. Ranges of $\delta^{15}N\text{-}NH_4^+$ from different sites(Pan et al., 2016; Kundu et al., 2010; Kawashima and Kurahashi, 2011) and different emission sources(Felix et al., 2013; Bhattarai et al., 2021; Chang et al., 2016; Xiao et al., 2020).

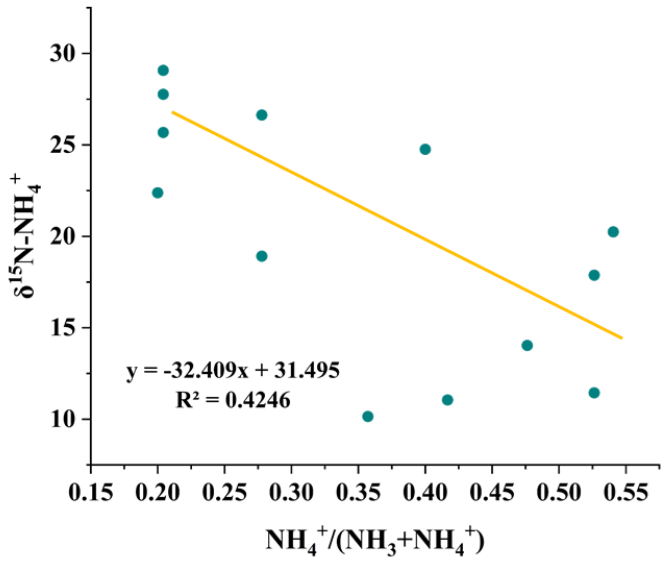

Figure S2. Linear fitting of $NH_4^+/(NH_3+NH_4^+)$ with $\delta^{15}N\text{-}NH_4^+$.

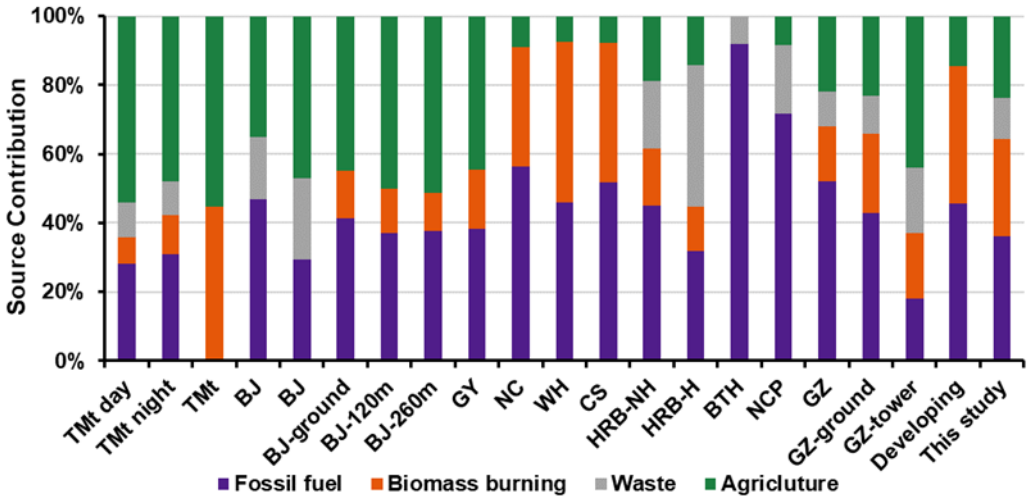

Figure S3. The comparison of sources apportionment results of atmospheric NH_3 and NH_4^+ in different sites in China. Background site in Tai mountain[TMt] (Wu et al., 2021; Chang et al., 2019), urban sites in North China (Beijing [BJ] (Pan et al., 2020; Chang et al., 2016), vertical profile observation in Beijing (ground, 120m height, and 260m height [BJ-ground, BJ-120m, and BJ-260m] (Wu et al., 2019), Jingjinji region [BTH] (Zhang et al., 2020), and North China plain [NCP]) (Xiang et al., 2022), East North China (Harbin heating period and non-heating period [HRB-H and HRB-NH]) (Sun et al., 2021), Central China (Wuhan [WH] and Changsha [CS]) (Xiao et al., 2020), East China (Nangchang [NC]) (Xiao et al., 2020), Southwest China (Guiyang [GY], source in precipitation) (Liu et al., 2017), and South China (Guangzhou[GZ]) (Liu et al., 2018), vertical profile observation in Guangzhou(ground and Guangzhou tower [GZ-ground and GZ-tower])(Chen et al., 2022). Source of NH_3 were estimated by inventory methods in developing country[developing] (Meng et al., 2017).

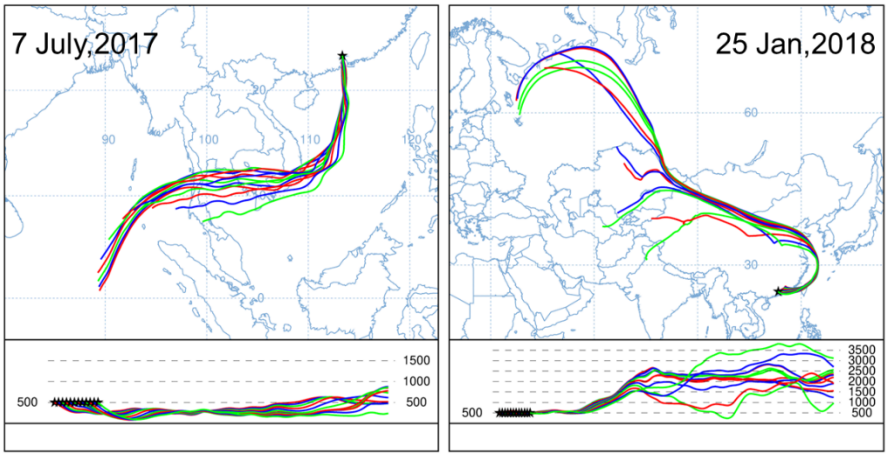

Figure S4. The air mass backward trajectory to receptor site on 7 July,2017 and 25 Jan,2018.

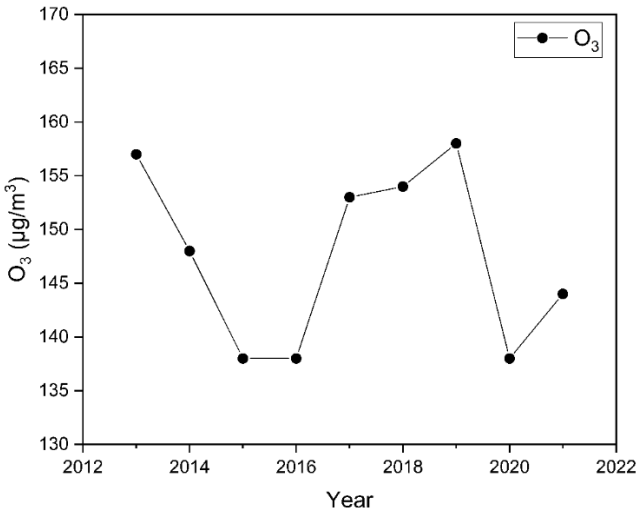

Figure S5. The temporal variation of O_3 concentration in PRD from 2013 to 2021.

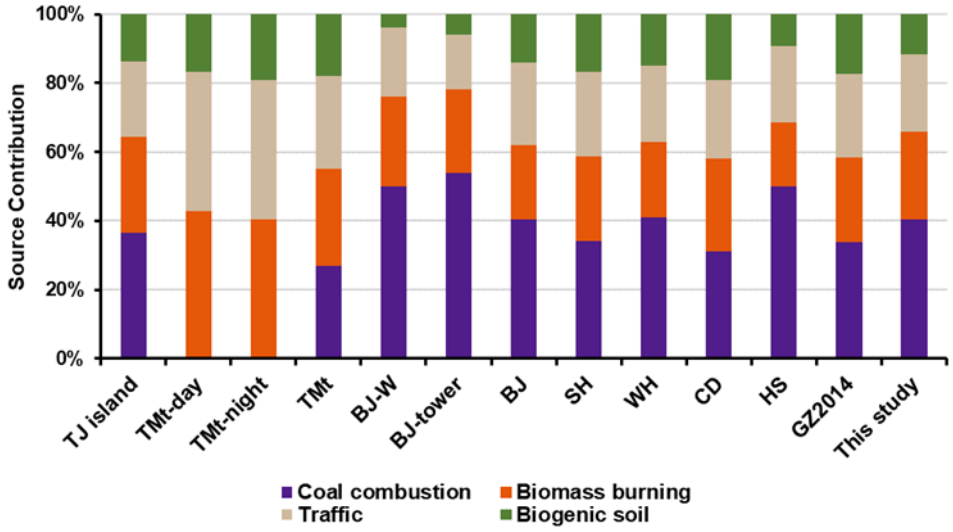

196

197 **Figure S6.** The comparison of sources apportionment results of atmospheric NOx and
198 NO_3^- in different sites in China. Background in Tuoji island [TJ island](Zong et al.,
199 2017) and Tai mountain [TMt] (Wu et al., 2021), urban sites in North China (Beijing
200 [BJ] (Zong et al., 2020), Beijing winter [BJ-W] (Fan et al., 2020), and vertical profile
201 observation in Beijing [BJ-tower](Fan et al., 2022)), Central China (Wuhan [WH])
202 (Zong et al., 2020), East China (Shanghai [SH]) (Zong et al., 2020), Southwest China
203 (Chengdu [CD]) (Zhang et al., 2022), and South China (Guangzhou [GZ2014])(Fan et
204 al., 2022).

References:

Bhattarai, N., Wang, S., Pan, Y., Xu, Q., Zhang, Y., Chang, Y., and Fang, Y.: delta(15)N-stable isotope analysis of NHx : An overview on analytical measurements, source sampling and its source apportionment, Front. Environ. Sci. Eng., 15, 126, https://doi.org/10.1007/s11783-021-1414-6, 2021.

Chang, Y., Liu, X., Deng, C., Dore, A. J., and Zhuang, G.: Source apportionment of atmospheric ammonia before, during, and after the 2014 APEC summit in Beijing using stable nitrogen isotope signatures, Atmos. Chem. Phys., 16, 11635-11647, https://doi.org/10.5194/acp-16-11635-2016, 2016.

Chang, Y., Zhang, Y.-L., Li, J., Tian, C., Song, L., Zhai, X., Zhang, W., Huang, T., Lin, Y.-C., Zhu, C., Fang, Y., Lehmann, M. F., and Chen, J.: Isotopic constraints on the atmospheric sources and formation of nitrogenous species in clouds influenced by biomass burning, Atmos. Chem. Phys., 19, 12221–12234, https://doi.org/10.5194/acp-19-12221-2019, 2019.

Chen, Z., Pei, C., Liu, J., Zhang, X., Ding, P., Dang, L., Zong, Z., Jiang, F., Wu, L., Sun, X., Zhou, S., Zhang, Y., Zhang, Z., Zheng, J., Tian, C., Li, J., and Zhang, G.: Non-agricultural source dominates the ammonium aerosol in the largest city of South China based on the vertical $\delta^{15}N$ measurements, Sci. Total Environ., 848, 157750, https://doi.org/10.1016/j.scitotenv.2022.157750, 2022.

Elliott, E. M., Kendall, C., Wankel, S. D., Burns, D. A., Boyer, E. W., Harlin, K., Bain, D. J., and Butler, T. J.: Nitrogen isotopes as indicators of NOx source contributions to atmospheric nitrate deposition across the midwestern and Northeastern United States, Environ. Sci. Technol., 41, 7661-7667, https://doi.org/10.1021/es070898t, 2007.

Fan, M.-Y., Zhang, Y.-L., Hong, Y., Lin, Y.-C., Zhao, Z.-Y., Cao, F., Sun, Y., Guo, H., and Fu, P.: Vertical differences of nitrate sources in urban boundary layer based on tower measurements, Environ. Sci. Technol. Lett., 2c00600, https://doi.org/10.1021/acs.estlett.2c00600, 2022.

Fan, M. Y., Zhang, Y. L., Lin, Y. C., Cao, F., Zhao, Z. Y., Sun, Y., Qiu, Y., Fu, P., and Wang, Y.: Changes of emission sources to nitrate aerosols in Beijing after the clean air actions: evidence from dual isotope compositions, J. Geophys. Res.: Atmos., 125, 031998, https://doi.org/10.1029/2019jd031998, 2020.

Fang, Y. T., Koba, K., Wang, X. M., Wen, D. Z., Li, J., Takebayashi, Y., Liu, X. Y., and Yoh, M.: Anthropogenic imprints on nitrogen and oxygen isotopic composition of precipitation nitrate in a nitrogen-polluted city in southern China, Atmos. Chem. Phys., 11, 1313-1325, https://doi.org/10.5194/acp-11-1313-2011, 2011.

Felix, J. D. and Elliott, E. M.: The agricultural history of human-nitrogen interactions as recorded in ice core $\delta^{15}N\text{-}NO_3^-$, Geophys. Res. Lett., 40, 1642-1646, https://doi.org/10.1002/grl.50209, 2013.

Felix, J. D., Elliott, E. M., and Shaw, S. L.: Nitrogen isotopic composition of coal-fired power plant NOx: influence of emission controls and implications for global emission inventories, Environ. Sci. Technol., 46, 3528-3535, https://doi.org/10.1021/es203355v, 2012.

Felix, J. D., Elliott, E. M., Gish, T. J., McConnell, L. L., and Shaw, S. L.: Characterizing the isotopic composition of atmospheric ammonia emission sources using passive samplers and a combined oxidation-bacterial denitrifier approach, Rapid Commun. Mass Spectrom., 27, 2239-2246, https://doi.org/10.1002/rcm.6679, 2013.

Felix, J. D., Elliott, E. M., Avery, G. B., Kieber, R. J., Mead, R. N., Willey, J. D., and Mullaugh, K. M.: Isotopic composition of nitrate in sequential Hurricane Irene precipitation samples: Implications for changing NOx sources, Atmos. Environ., 106, 191-195, https://doi.org/10.1016/j.atmosenv.2015.01.075, 2015.

Fibiger, D. L. and Hastings, M. G.: First Measurements of the Nitrogen Isotopic Composition of NOx

from Biomass Burning, Environ. Sci. Technol., 50, 11569-11574, https://doi.org/10.1021/acs.est.6b03510, 2016.

Hastings, M. G., Sigman, D. M., and Lipschultz, F.: Isotopic evidence for source changes of nitrate in rain at Bermuda, J. Geophys. Res.: Atmos., 108, 1-12, https://doi.org/10.1029/2003jd003789, 2003.

Jiang, H., Li, J., Sun, R., Liu, G., Tian, C., Tang, J., Cheng, Z., Zhu, S., Zhong, G., Ding, X., and Zhang, G.: Determining the sources and transport of brown carbon using radionuclide tracers and modeling, J. Geophys. Res.: Atmos., 126, e2021JD034616, https://doi.org/10.1029/2021jd034616, 2021.

Kawashima, H. and Kurahashi, T.: Inorganic ion and nitrogen isotopic compositions of atmospheric aerosols at Yurihonjo, Japan: implications for nitrogen sources, Atmos. Environ., 45, 6309-6316, https://doi.org/10.1016/j.atmosenv.2011.08.057, 2011.

Kundu, S., Kawamura, K., and Lee, M.: Seasonal variation of the concentrations of nitrogenous species and their nitrogen isotopic ratios in aerosols at Gosan, Jeju Island: Implications for atmospheric processing and source changes of aerosols, J. Geophys. Res. , 115, https://doi.org/10.1029/2009jd013323, 2010.

Liao, B., Wu, D., Chang, Y., Lin, Y., Wang, S., and Li, F.: Characteristics of particulate SO_4^{2-}, NO_3^-, NH_4^+, and related gaseous pollutants in Guangzhou (in Chinese), Acta Sci. Circumst., 34, 1551-1559, https://doi.org/10.13671/j.hjkxxb.2014.0218, 2014.

Liu, G., Wu, J., Li, Y., Su, L., and Ding, M.: Temporal variations of ^{7}Be and ^{210}Pb activity concentrations in the atmosphere and aerosol deposition velocity in Shenzhen, South China, Aerosol Air Qual. Res., 20, 1607–1617, https://doi.org/10.4209/aaqr.2019.11.0560, 2020.

Liu, J., Ding, P., Zong, Z., Li, J., Tian, C., Chen, W., Chang, M., Salazar, G., Shen, C., Cheng, Z., Chen, Y., Wang, X., Szidat, S., and Zhang, G.: Evidence of rural and suburban sources of urban haze formation in China: a case study from the Pearl River Delta region, J. Geophys. Res.: Atmos., 123, 4712-4726, https://doi.org/10.1029/2017jd027952, 2018.

Liu, X. Y., Xiao, H. W., Xiao, H. Y., Song, W., Sun, X. C., Zheng, X. D., Liu, C. Q., and Koba, K.: Stable isotope analyses of precipitation nitrogen sources in Guiyang, southwestern China, Environ. Pollut., 230, 486-494, https://doi.org/10.1016/j.envpol.2017.06.010, 2017.

Martinellia, L. A., Camargoa, P. B., Laraa, L. B. L. S., Victoriaa, R. L., and Artaxo, P.: Stable carbon and nitrogen isotopic composition of bulk aerosol particles in a C4 plant landscape of southeast Brazil, Atmos. Environ., 36, 2427–2432, https://doi.org/10.1016/S1352-2310(01)00454-X, 2002.

Meng, W., Zhong, Q., Yun, X., Zhu, X., Huang, T., Shen, H., Chen, Y., Chen, H., Zhou, F., Liu, J., Wang, X., Zeng, E. Y., and Tao, S.: Improvement of a global high-resolution ammonia emission inventory for combustion and industrial sources with new data from the residential and transportation sectors, Environ. Sci. Technol., 51, 2821-2829, https://doi.org/10.1021/acs.est.6b03694, 2017.

Pan, Y., Tian, S., Liu, D., Fang, Y., Zhu, X., Zhang, Q., Zheng, B., Michalski, G., and Wang, Y.: Fossil fuel combustion-related emissions dominate atmospheric ammonia sources during severe haze episodes: evidence from ^{15}N-stable isotope in size-resolved aerosol ammonium, Environ. Sci. Technol., 50, 8049-8056, https://doi.org/10.1021/acs.est.6b00634, 2016.

Pan, Y., Gu, M., He, Y., Wu, D., Liu, C., Song, L., Tian, S., Lü, X., Sun, Y., Song, T., Walters, W. W., Liu, X., Martin, N. A., Zhang, Q., Fang, Y., Ferracci, V., and Wang, Y.: Revisiting the concentration observations and source apportionment of atmospheric ammonia, Adv. Atmos. Sci., 37, 933-938, https://doi.org/10.1007/s00376-020-2111-2, 2020.

Sun, X., Zong, Z., Li, Q., Shi, X., Wang, K., Lu, L., Li, B., Qi, H., and Tian, C.: Assessing the emission sources and reduction potential of atmospheric ammonia at an urban site in Northeast China, Environ.

Res., 198, 111230, https://doi.org/10.1016/j.envres.2021.111230, 2021.
Walters, W. W., Tharp, B. D., Fang, H., Kozak, B. J., and Michalski, G.: Nitrogen Isotope Composition of Thermally Produced NOx from Various Fossil-Fuel Combustion Sources, Environ. Sci. Technol., 49, 11363-11371, https://doi.org/10.1021/acs.est.5b02769, 2015.
Walters, W. W., Song, L., Chai, J., Fang, Y., Colombi, N., and Hastings, M. G.: Characterizing the spatiotemporal nitrogen stable isotopic composition of ammonia in vehicle plumes, Atmos. Chem. Phys., 20, 11551-11567, https://doi.org/10.5194/acp-20-11551-2020, 2020.
Wu, L., Yue, S., Shi, Z., Hu, W., Chen, J., Ren, H., Deng, J., Ren, L., Fang, Y., Li, W., Harrison, R. M., and Fu, P.: Source forensics of inorganic and organic nitrogen using δ15N for tropospheric aerosols over Mt. Tai, npj Clim. Atmos. Sci., 8, https://doi.org/10.1038/s41612-021-00163-0, 2021.
Wu, L., Ren, H., Wang, P., Chen, J., Fang, Y., Hu, W., Ren, L., Deng, J., Song, Y., Li, J., Sun, Y., Wang, Z., Liu, C.-Q., Ying, Q., and Fu, P.: Aerosol ammonium in the urban boundary layer in Beijing: insights from nitrogen isotope ratios and simulations in summer 2015, Environ. Sci. Technol. Lett., 6, 389-395, https://doi.org/10.1021/acs.estlett.9b00328, 2019.
Xiang, Y.-K., Dao, X., Gao, M., Lin, Y.-C., Cao, F., Yang, X.-Y., and Zhang, Y.-L.: Nitrogen isotope characteristics and source apportionment of atmospheric ammonium in urban cities during a haze event in Northern China Plain, Atmos. Environ., 269, 118800, https://doi.org/10.1016/j.atmosenv.2021.118800, 2022.
Xiao, H.-W., Xie, L.-H., Long, A.-M., Ye, F., Pan, Y.-P., Li, D.-N., Long, Z.-H., Chen, L., Xiao, H.-Y., and Liu, C.-Q.: Use of isotopic compositions of nitrate in TSP to identify sources and chemistry in South China Sea, Atmos. Environ., 109, 70-78, https://doi.org/10.1016/j.atmosenv.2015.03.006, 2015.
Xiao, H. W., Wu, J. F., Luo, L., Liu, C., Xie, Y. J., and Xiao, H. Y.: Enhanced biomass burning as a source of aerosol ammonium over cities in central China in autumn, Environ. Pollut., 266, 115278, https://doi.org/10.1016/j.envpol.2020.115278, 2020.
Zhang, Z., Zeng, Y., Zheng, N., Luo, L., Xiao, H., and Xiao, H.: Fossil fuel-related emissions were the major source of NH_3 pollution in urban cities of northern China in the autumn of 2017, Environ. Pollut., 256, 113428, https://doi.org/10.1016/j.envpol.2019.113428, 2020.
Zhang, Z., Zhu, W., Hu, M., Wang, H., Tang, L., Hu, S., Shen, R., Yu, Y., Song, K., Tan, R., Chen, Z., Chen, S., Canonaco, F., Prevot, A. S. H., and Guo, S.: Secondary organic aerosol formation in China from urban-lifestyle sources: Vehicle exhaust and cooking emission, Sci. Total Environ., 857, 159340, https://doi.org/10.1016/j.scitotenv.2022.159340, 2022.
Zong, Z.: Composition and source apportionment of $PM_{2.5}$ at the background area in North China, Doctor, Yantai Institute of Coastal Zone Research, Chinese Academy of Sciences, 2017.
Zong, Z., Shi, X., Sun, Z., Tian, C., Li, J., Fang, Y., Gao, H., and Zhang, G.: Nitrogen isotopic composition of NOx from residential biomass burning and coal combustion in North China, Environ. Pollut., 304, 119238, https://doi.org/10.1016/j.envpol.2022.119238, 2022.
Zong, Z., Tan, Y., Wang, X., Tian, C., Li, J., Fang, Y., Chen, Y., Cui, S., and Zhang, G.: Dual-modelling-based source apportionment of NOx in five Chinese megacities: providing the isotopic footprint from 2013 to 2014, Environ. Int., 137, 105592, https://doi.org/10.1016/j.envint.2020.105592, 2020.
Zong, Z., Wang, X., Tian, C., Chen, Y., Fang, Y., Zhang, F., Li, C., Sun, J., Li, J., and Zhang, G.: First assessment of NOx sources at a regional background site in North China using isotopic analysis linked with modeling, Environ. Sci. Technol., 51, 5923-5931, https://doi.org/10.1021/acs.est.6b06316, 2017.